

Reinvestigation of the electron fraction and electron Fermi energy of neutron star

Z.-F. Gao^{1,2,*}, H. Shan¹, W. Wang³, and N. Wang^{1,**}

¹ Xinjiang Astronomical Observatory, CAS, 150, Science 1-Street, Urumqi, Xinjiang, 830011, China

² Key Laboratory of Radio Astronomy, Chinese Academy of Sciences, West Beijing Road, Nanjing, 210008, China

³ School of Physics and Technology, Wuhan University, Wuhan, Hubei, 430072, China

Received 5 June 2017, accepted 30 August 2017

Published online later

Key words Neutron star–Equation of state– Electron Fermi energy

In this work, we reinvestigate the electron fraction Y_e and electron Fermi energy $E_F(e)$ of neutron stars, based on our previous work, in which we firstly deduced a special solution to $E_F(e)$, and then obtained several useful analytical formulae for Y_e and matter density ρ within classical models and the relativistic mean field (RMF) theory using numerically fitting. The advantages of this work include the following aspects: (1) The linear functions are substituted for the nonlinear exponential functions used in the previous work. This method may be more simple, and closer to realistic equation of state (EoS) of a neutron star (NS), because there are linear or quasi-linear relationships between number fractions of leptons and matter density, which can be seen by solving NS EoS; (2) we introduce a dimensionless variable ϱ ($\varrho = \rho/\rho_0$, ρ_0 is the standard saturated nuclear density), which greatly reduces the scope of the fitting coefficients; (3) we present numerical errors including absolute and relative deviations between the data and fit. By numerically simulating, we have obtained several analytical formulae for Y_e and ρ for both APR98 and RMF models. Combining these analytical formulae with the special solution, we can calculate the value of $E_F(e)$ for any given matter density. Since Y_e and $E_F(e)$ are important in assessing cooling rate of a NS and the possibility of kaon/pion condensation in the NS interior, this study could be useful in the future study on the thermal evolution of a NS.

© 2006 WILEY-VCH Verlag GmbH & Co. KGaA, Weinheim

1 Introduction

Neutron star (NS) constitutes one of the best astro-physical laboratories for studying dense matter physics. An equation of state (EoS) of matter under exotic conditions is a prerequisite for studies of the structure and evolution of compact stars. As an extremely interesting and important physical parameter in NS EoS, the electron fraction, Y_e , influences on the weak-interactions processes, e.g., modified Urca reactions, α -decay, electron capture as well as the absorption of neutrinos and anti-neutrinos, and etc (see Yakovlev et al. 2001; Dong et al. 2013, 2016; Gao et al. 2011a, 2011b, Liu & Liu 2017a, 2017b; Liu et al. 2017a, 2017b; Sun et al. 2016; Cheng et al. 2015, 2017a, 2017b). The electron fraction Y_e is defined as $Y_e = n_e/n_B$, and varies with matter density, where n_e and n_B are the electron number density and baryon number density, respectively. For a given NS matter density, how to exactly determine the values of Y_e has long been a very challenging task for both the nuclear physics and astrophysics community, due to some uncertainties and artificial assumptions. Currently, our knowledge of Y_e mainly comes from model-dependent EoS of a NS (e.g., Baym, Pethick & Sutherland 1971; Douchin &

Haensel 2000, 2001; Lattimer & Prakash 2007; Kaminker et al. 2014; Gomes et al. 2014, 2017; Graber et al. 2015, 2017).

The other important parameter is the electron Fermi energy, $E_F(e)$, which denotes the highest energy of electron gas. As we know, for degenerate and relativistic electrons in β -equilibrium, the distribution function $f(E_e)$ obeys Fermi-Dirac statistics, and the electron chemical potential μ_e at zero-temperature is called its Fermi energy. In the weak-magnetic field limit, $B \ll B_{cr}$ (B_{cr} is the electron critical magnetic field), the isoenergetic surface of degenerate and relativistic electrons is a spherical surface in the momentum space. The Fermi energy of electrons inside a NS can exert directly impact not only on the weak-interactions processes, but also on the electron degeneracy pressure counteracting gravity collapse of the star. These impacts will in turn change intrinsic EoS (e.g., Gao et al. 2015; Liu 2016; Zhu et al. 2016), internal structure and heat evolution, and even influence the whole properties of the star. Thus, more attention has been paid to the two parameters above due to their importance.

Our previous work of Li et al. (2016) (“Li16” in short) is devoted to consideration of the electron Fermi energy and an associated value of electron number fraction as functions of matter density ρ within different layers of neutron star’s crust and core of a common NS with $B \ll B_{cr}$ (Li et al. 2016; Gao et al. 2017). Since the main purpose of this paper

* Corresponding author: e-mail: zhifugao@xao.ac.cn

** Corresponding author: e-mail: na.wang@xao.ac.cn

is to reinvestigate Y_e and $E_F(e)$ inside a NS by revising Li16, it is necessary to briefly review Li16. Please see below for details.

(i) Based on the basic definition of the Fermi energy of degenerate and relativistic electrons, we deduced a special solution to the electron Fermi energy,

$$E_F(e) = 60 \times \left(\frac{\rho}{\rho_0}\right)^{1/3} \left(\frac{Y_e}{0.005647}\right)^{1/3} \text{ (MeV)}. \quad (1)$$

which is suitable for relativistic electron matter region ($\rho \geq 10^7 \text{ g cm}^{-3}$) in a common NS. Here $\rho_0 = 2.8 \times 10^{14} \text{ g cm}^{-3}$ is the standard nuclear density.

(ii) According to generally accepted and reliable EoSs of a NS, we obtained several useful analytical formulae for Y_e and matter density ρ within classical matter models and the work of Dutra et al. (2014)(Type-2) in relativistic mean field (RMF) theory.

(iii) Since $E_F(e)$ and Y_e are smooth and continuous functions of ρ , we plot the diagrams of $E_F(e)$ vs. ρ and Y_e vs. ρ using the fitting formula of $E_F(e)$, Y_e and ρ in four matter regions (the outer crust, inner crust, outer core, and inner core) and some boundary conditions.

(iv) When describing the mean-field Lagrangian, density, we adopted the TMA parameter set, which aims at a consistent description of all the nuclei with one parameter set and is remarkably consistent with the updated astrophysical observations of NSs. Due to the importance of the density dependence of symmetry energy, J , in nuclear astrophysics, a brief discussion on J and its slop was presented.

(v) Compared with previous studies on the electron Fermi energy in other models, the methods of calculating $E_F(e)$ in Li16 are more simple and convenient. Since Urca reactions are expected in the center of a massive star due to high-value $E_F(e)$ and Y_e , the work of Li16 could be useful in the future studies on the NS thermal evolution.

It must be said that our endeavors in Li16 are indeed of practical use for exploring efficiently many properties of NSs, especially if the fits are in a compact and widely applicable form. Recently, after a careful examination, we found some inadequacies of Li16, which should be improved significantly. See below for details.

(i) The electron fractions in Li16 have in fact in all cases expressed as second or third order polynomials in the natural exponential function of $e^{\text{Log}_{10}\rho}$, which leads to an extremely wide coefficient range. Such a wide range of coefficients indeed limits their applicability. It can be implemented by solving a linear system instead of the more involved non-linear optimization problem needed for expressions like Eq.(9) of Potekhin et al. (2013).

(ii) No mention to the errors in the fit parameters is presented in Li16. Although our fit quality is indeed so good that all significant digits in Li16 are basically correct and the fitted errors can be neglected.

Based on the analysis above, we will reinvestigate the fraction and Fermi energy of relativistic electrons inside a common NS. We will perform numerical simulations in APR98 model in section 2, and in RMF models in section 3. The main conclusions are given in section 4.

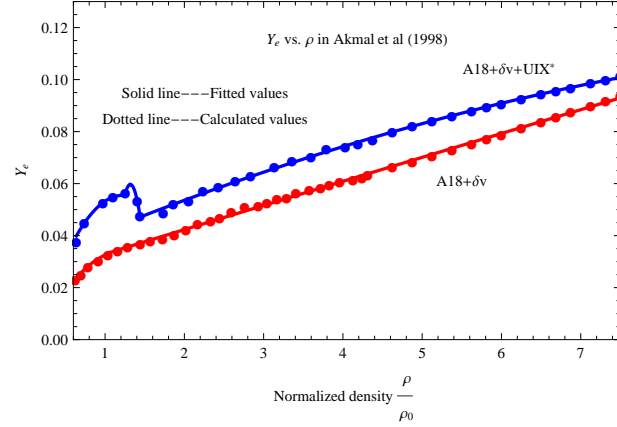


Fig. 1 Comparisons of the data and fits for Y_e as a function of ρ for for A18 + δv and Av18 + δv + UIX* models in APR 1998.

2 Numerical Simulations in the APR98 model

Employing Argonne v18 two-nucleon (Av18) interaction and variational chain summation methods, Akmal, Pandharipande, & Ravenhall(1998) (“APR98”) investigated the properties of dense nucleon matter and the structure of NSs, and provided an excellent fit to all of the nucleon-nucleon scattering data in the Nijmegen data base (Stoks et al. 1993). In APR98, the authors not only considered the non-relativistic calculations with Av18 and Av18+UIX (Urbana IX three-nucleon interaction) models for nuclear forces, but also described the relativistic boost interaction model (denoted as δv) with and without three-nucleon interaction (UIX*). The difference between Av18+ δv and Av18+ δv +UIX* models lies in that whether the effect of three-nucleon interaction (TNI) is considered. Here we will choose Av18+ δv and Av18+ δv +UIX* as two representative models in the following simulations because these two models can be regarded as more realistic models.

According to the APR98, the effective interactions have same form

$$H = \left[\frac{\hbar^2}{2m} + (p_3 + (1 - Y_p)p_5)\rho e^{-p_4\rho}\right] \tau_n + \left[\frac{\hbar^2}{2m} + (p_3 + Y_p p_5)\rho e^{-p_4\rho}\right] \tau_p + g(\rho, Y_p = 0.5) (1 - (1 - 2Y_p)^2) + g(\rho, Y_p = 0)(1 - 2Y_p)^2, \quad (2)$$

where $\rho = \rho_n + \rho_p$ at zero temperature, and

$$\tau_p = \frac{3}{5} (3\pi^2 \rho)^{\frac{2}{3}} Y_p^{\frac{5}{3}}, \tau_n = \frac{3}{5} (3\pi^2 \rho)^{\frac{2}{3}} (1 - Y_p)^{\frac{5}{3}}. \quad (3)$$

The parameters defining the τ -dependent terms are the same for the two models, and are given in APR98. For Av18+ δv and three-nucleon interaction models at the low-density phase, the parametrization $g_L(Y_p)$ is expressed as

$$g_L(\rho, Y_p = 0.5) = -\rho^2 (p_1 + p_2 \rho + p_6 \rho^2 + (p_{10} + p_{11} \rho) e^{-p_9^2 \rho^2}),$$

$$g_L(\rho, Y_p = 0) = -\rho^2(p_{12}/\rho + p_7 + p_8\rho + p_{13} e^{-p_9^2\rho^2}), \quad (4)$$

while at the high-density phase, the parameter $g_H(Y_p)$ is written as

$$\begin{aligned} g_H(Y_p = 0.5) &= g_L(Y_p = 0.5) - \rho^2(p_{17}(\rho - p_{19}) + p_{21}(\rho - p_{19})^2) e^{p_{18}(\rho - p_{19})}, \\ g_H(Y_p = 0) &= g_L(Y_p = 0) - \rho^2(p_{15}(\rho - p_{20}) + p_{14}(\rho - p_{20})^2) e^{p_{16}(\rho - p_{20})}. \end{aligned} \quad (5)$$

The parameter values of $P_j, i = 1, 2, \dots, 21$ are listed in Table 1. Here, the parameters $p_3 = 89.8 \text{ MeV fm}^5$, $p_4 = 0.457 \text{ fm}^3$ and $p_5 = -59.0 \text{ MeV fm}^5$ are common to these two models.

Table 2 lists partial values of n_B, ρ, Y_e and $E_F(e)$. In order to reduce the scope of coefficients of fitted polynomial expressions of Y_e and ρ for $A18+\delta v$ and $Av18+\delta v+UIX^*$ models, let us introduce a dimensionless variable ϱ ($\varrho = \rho/\rho_0$, ρ_0 is the standard saturated nuclear density), which is the order of close to unity, and adopt a new form of $\sum_{n=0}^{n_{\max}} c_n \varrho^n$, where c_n is the n -th order coefficient of the fitted polynomial expression. As to the $Av18+\delta v+UIX^*$ model, the original data of Y_e are divided into three groups with consideration of variation tendency. By performing 2nd order polynomial fitting, we obtain

$$\begin{aligned} Y_e &= -0.01232 + 0.1184 \varrho - 0.0572 \varrho^2, \\ Y_e &= -1.4321 + 2.3246 \varrho - 0.9085 \varrho^2, \\ Y_e &= 0.0291 + 0.0146 \varrho - 5.68 \times 10^{-4} \varrho^2, \end{aligned} \quad (6)$$

for $\varrho \sim 0.59 - 1.19$ ($\rho \sim (1.66 \times 10^{14} - 3.331 \times 10^{14}) \text{ g cm}^{-3}$), $\varrho \sim 1.190 - 1.37$ ($\rho \sim (3.33 \times 10^{14} - 3.83 \times 10^{14}) \text{ g cm}^{-3}$), and $\varrho \sim 1.37 - 7.12$ ($\rho \sim (3.83 \times 10^{14} - 1.99 \times 10^{15}) \text{ g cm}^{-3}$), respectively, where $n_{\max} = 2$ is assumed. When at the density-node of $\varrho = 1.19$, the ‘‘jump’’ of Y_e is 0.0007, corresponding to a relative variation $|\Delta Y_e/Y_e| \sim 1.4\%$, while at the point $\varrho = 1.366$, the ‘‘jump’’ is about 0.0006, corresponding to a relative variation of 1.2%. Thus, the continuities of three functionals in Equation (6) are enforced. The comparisons between the data and the fit show that the residuals of Y_e are typically 10^{-4} , the relative differences are smaller than 3%.

3 Numerical simulations in the RMF models

To date, many of relativistic models have drawn attentions in investigating NS EoSs (e.g., Glendenning et al. 1985; Schaffner & Mishustin 1996; Zhou et al. 2017; Mu et al. 2017). The most common among them is the RMF theory, which has become standard method to study nuclear matter and finite-nuclei properties. According to RMF models, the strong interaction between baryons is mediated by the exchange of isoscalar scalar and vector mesons σ, ω , isovector vector meson ρ . There are two additional strange mesons namely isoscalar scalar σ^* and vector ϕ mesons considered by some authors (e.g., Yang & Shen 2008; Xu et al. 2012;

Zhao 2015, 2016). The total effective Lagrangian is given by

$$\begin{aligned} L &= \sum_B \bar{\psi}_B [i\gamma_\mu \partial^\mu - (m_B - g_{\sigma B} \sigma - g_{\sigma^* B} \sigma^*) - g_{\rho B} \gamma_\mu \tau \cdot \rho^\mu - g_{\omega B} \gamma_\mu \omega^\mu - g_{\phi B} \gamma_\mu \phi^\mu] \psi_B + \frac{1}{2} (\partial_\mu \sigma \partial^\mu \sigma - m_\sigma^2 \sigma^2) + \frac{1}{2} (\partial_\nu \sigma^* \partial^\nu \sigma^* - m_{\sigma^*}^2 \sigma^{*2}) \\ &\quad - \frac{1}{4} W^{\mu\nu} W_{\mu\nu} - \frac{1}{4} R^{\mu\nu} R_{\mu\nu} + \frac{1}{2} m_\rho^2 \rho_\mu \rho^\mu - \frac{1}{4} P^{\mu\nu} P_{\mu\nu} + \frac{1}{2} m_\omega^2 \omega_\mu \omega^\mu - \frac{1}{3} a \sigma^3 - \frac{1}{4} b \sigma^4 + \frac{1}{2} m_\phi^2 \phi_\mu \phi^\mu \\ &\quad + \frac{1}{4} c_3 (\omega_\mu \omega^\mu)^2 + \sum_l \bar{\psi}_l [i\gamma_\mu \partial^\mu - m_l] \psi_l. \end{aligned} \quad (7)$$

where $W_{\mu\nu} = \partial_\mu \omega_\nu - \partial_\nu \omega_\mu$, $R_{\mu\nu} = \partial_\mu \rho_\nu - \partial_\nu \rho_\mu$ and $P_{\mu\nu} = \partial_\mu \phi_\nu - \partial_\nu \phi_\mu$ denote the field tensors of ω, ρ and ϕ mesons, respectively, and γ_μ is the Dirac matrix. The meson field equations in uniform matter have the following form

$$\begin{aligned} \sum_B g_{\sigma B} \rho_{SB} &= m_\sigma^2 \sigma + a \sigma^2 + b \sigma^3, \quad \sum_B g_{\omega B} \rho_B \\ &= m_\omega^2 \omega_0 + c_3 \omega_0^3, \quad \sum_B g_{\rho B} \rho_B I_{3B} = m_\rho^2 \rho_0, \\ \sum_B g_{\sigma^* B} \rho_{SB} &= m_{\sigma^*}^2 \sigma^*, \quad \sum_B g_{\phi B} \rho_B = m_\phi^2 \phi_0, \end{aligned} \quad (8)$$

where J_B and I_{3B} express the baryon spin and isospin projections, respectively. m_B^* is the baryon effective mass

$$m_B^* = m_B - g_{\sigma B} \cdot \sigma - g_{\sigma^* B} \cdot \sigma^*, \quad (9)$$

At zero temperature the lepton chemical potentials are expressed as

$$\mu_l = \sqrt{k_F^l{}^2 + m_l^2}, \quad (\text{fm}^{-1}). \quad (10)$$

The charge neutrality condition is given by

$$\sum_B q_B \rho_B - n_e - n_\mu = 0, \quad (11)$$

where $\sum_B q_B = n_B$, and q_B is the baryon electric charge. The coupled equations can be solved self-consistently.

In order to numerically simulate in RMF models, we select three representative parameter-set groups: NL3, TMA and GM1(SU3). The former two include three mesons: σ, ω and ρ , while the latter one includes $\sigma, \omega, \rho, \sigma^*$ and ϕ . These three RMF parameter-set group are successful in describing NS matter to some extent (Glendenning 1985; Lalazisis et al. 1995; Toki et al. 1995; Geng et al. 2005).

The saturation properties including mass parameters, meson-nucleon couplings and self-coupling constants of three RMF parameter sets are listed in Table 3.

In Table 3, ρ_0 is the saturation density, $E_0 = (E/A)_\infty$ is the bulk binding energy/nucleon, K_0 is the incompressibility, $m^* = M^*/M$ is the effective mass ratio, $K^r = -Q_0$ (Q_0 is the skewness coefficient), J is the symmetry energy at $\rho = \rho_0$, L_0 is the slope of the symmetry energy (S), K_{sym}^0 is the curvature of S , Q_{sym}^0 is the skewness of S and $K_{\tau,V}^0$ is the volume part of the isospin incompressibility.

Table 1 Partial values of n_B , ρ , Y_e and $E_F(e)$ for $Av18 + \delta v + UIX^*$ and $Av18 + \delta v$ models.

Model	P_1	P_2	P_6	P_7	P_8	P_9	P_{10}	P_{11}	P_{12}	P_{13}
$Av18+\delta v+UIX^*$	337.2	-382.0	-19.1	214.6	-384.0	6.4	69.0	-33.0	0.35	0
$A18+\delta v$	281.0	-151.1	-10.6	210.1	-158.0	5.88	58.8	-15.0	-0.2	-0.9
Model	p_{14}	p_{15}	p_{16}	p_{17}	p_{18}	p_{19}	p_{20}	p_{21}	--	--
$Av18+\delta v+UIX^*$	0	287.0	-1.54	175.0	-1.45	0.32	0.195	0	--	--

Table 2 Partial values of n_B , ρ , Y_e and $E_F(e)$ for $Av18 + \delta v + UIX^*$ and $Av18 + \delta v$ models.

n_B (fm^{-3})	Matter-density (g cm^{-3})	Y_e (%)	$E_F(e)$ (MeV)	$E_F^\dagger(e)$ (MeV)	n_B (fm^{-3})	Matter-density (g cm^{-3})	Y_e (%)	$E_F(e)$ (MeV)	$E_F^\dagger(e)$ (MeV)
<i>Av18 + δv</i>									
0.10	1.661×10^{14}	2.395	81.60	81.32	0.67	1.113×10^{15}	6.237	211.64	211.96
0.17	2.178×10^{14}	2.789	102.45	102.19	0.74	1.229×10^{15}	6.620	223.15	223.33
0.23	3.819×10^{14}	3.683	124.33	124.03	0.82	1.362×10^{15}	7.068	236.02	236.32
0.30	4.982×10^{14}	4.165	141.52	141.02	0.90	1.495×10^{15}	7.528	248.63	248.76
0.37	6.144×10^{14}	4.590	156.76	156.76	0.96	1.594×10^{15}	7.881	257.95	258.21
0.41	6.808×10^{14}	4.820	164.88	164.56	1.00	1.661×10^{15}	8.121	264.11	264.43
0.45	7.473×10^{14}	5.043	172.67	172.36	1.04	1.727×10^{15}	8.365	270.23	270.65
0.49	8.137×10^{14}	5.262	180.17	180.10	1.07	1.777×10^{15}	8.552	274.23	274.54
0.57	9.465×10^{14}	5.695	194.55	194.67	1.14	1.893×10^{15}	8.991	285.42	285.56
0.64	1.063×10^{15}	6.073	206.59	206.65	1.20	1.993×10^{15}	9.378	294.45	294.64
<i>A18 + $\delta v + UIX^*$</i>									
0.10	1.661×10^{14}	3.707	94.38	94.09	0.67	1.113×10^{15}	7.633	226.38	226.65
0.17	2.178×10^{14}	4.701	121.94	121.38	0.74	1.229×10^{15}	8.001	237.71	237.93
0.23	3.819×10^{14}	4.791	135.72	135.25	0.82	1.362×10^{15}	8.404	250.04	250.21
0.30	4.982×10^{14}	5.274	153.11	152.81	0.90	1.495×10^{15}	8.789	261.99	262.23
0.37	6.144×10^{14}	5.796	169.44	169.17	0.96	1.594×10^{15}	9.068	270.29	270.65
0.41	6.808×10^{14}	6.073	178.09	177.88	1.00	1.661×10^{15}	9.251	275.84	275.99
0.45	7.473×10^{14}	6.385	186.33	186.01	1.04	1.727×10^{15}	9.429	280.26	280.54
0.49	8.137×10^{14}	6.592	194.23	194.03	1.07	1.777×10^{15}	9.563	285.26	285.76
0.57	9.465×10^{14}	7.073	209.12	209.37	1.14	1.893×10^{15}	9.864	294.37	294.57
0.64	1.063×10^{15}	7.468	221.54	221.33	1.20	1.993×10^{15}	10.12	301.98	302.46

Footnote: \dagger . Calculated values of $E_F(e)$ by combining Eq.(1) with the fitted polynomial expressions of Eqs.(6-7).

Table 3 Saturation properties, meson-nucleon couplings and self-coupling constants of three RMF models.

Model	ρ_0 fm^{-3}	E_0 MeV	K_0 MeV	m^*	K' MeV	J MeV	L_0 MeV	K_{sym}^0 MeV	Q_{sym}^0 MeV	$K_{\tau,V}^0$ MeV
NL3	0.148	-16.24	271.53	0.60	-202.91	37,40	118.53	100.88	181.31	-698.85
TMA	0.147	-16.02	318.15	0.635	572.12	30.66	90.14	10.75	-108.74	-367.99
GM1(SU3)	0.153	-16.33	300.50	0.70	215.66	32.52	94.02	17.98	25.01	-478.64
Model	m_N MeV	m_σ MeV	m_ω MeV	m_ρ MeV	$g_{\sigma N}$ fm^{-1}	$g_{\omega N}$ fm^{-1}	$g_{\rho N}$ fm^{-1}	a fm^{-1}	b fm^{-1}	c_3 fm^{-1}
NL3	939.0	508.194	782.50	763.0	10.217	12.868	4.474	-10.431	-28.885	0
TMA	939.0	519.151	781.95	768.1	10.055	12.842	3.800	-0.328	38.862	151.590
GM1(SU3) \dagger	938.0	550	783.0	770.0	4.10	10.26	4.10	12.28	-8.98	0

Footnote: \dagger . For the GM1(SU3) parameter set, the meson masses $m_{\sigma^*} = 975.0$ MeV, and $m_{\phi^*} = 1020.0$ MeV, the meson- hyperon couplings $g_{\sigma\Lambda} = 6.170 \text{ fm}^{-1}$, $g_{\sigma\Xi} = 1020.0 \text{ fm}^{-1}$, $g_{\sigma^*\Lambda} = 5.412 \text{ fm}^{-1}$, and $g_{\sigma^*\Lambda} = 11.516 \text{ fm}^{-1}$.

Inserting the parameter values of TMA into the standard procedure of RMF models, we calculate the values of the related quantities for TMA parameter set. By fitting, we obtain the analytical representations of Y_e and ρ in TMA model

$$Y_e = -0.00316 + 0.05258 \rho - 0.00514 \rho^2,$$

$$Y_e = 0.08235 + 0.0124 \rho - 5.04 \times 10^{-4} \rho^2, \quad (12)$$

for $\rho \sim (6.92 \times 10^{11} - 9.38 \times 10^{14})$ and $(9.38 \times 10^{14} - 2.69 \times 10^{15}) \text{ g cm}^{-3}$, respectively. At the midpoint of $2.98 \times 10^{14} \text{ g cm}^{-3}$, the "jump" of Y_e is about 2.8×10^{-3} , and its relative variation $\sim 2.5\%$ confirming the continuities of two expressions above. The typical differences between

the fit and the data are $10^{-3} - 10^{-4}$, and their relative differences are typically $10^{-2} - 10^{-3}$. The maximum absolute deviation and relative error are 4.5×10^{-3} and 3%, respectively, at the high-density end, due to uncertainty of the EoS. Combining Equation (12) with Equation (1), we can calculate the value of $E_F(e)$ in any given matter density for TMA parameter set. The comparisons of the EoS and its analytical expressions are shown in Figure 2(a) and (b). For the GM1(SU3) parameter set, the relation $g_{\sigma^*N} = g_{\rho\Lambda} = 0$ is assumed. Inserting the parameter values of GM1(SU3) into the standard procedure of RMF models, we calculate the values of n_B , n_e , Y_e and $E_F(e)$. By fitting, we obtain the

analytical representations of Y_e and ρ in GM1(SU3) model

$$\begin{aligned} Y_e &= -0.00298 + 0.0526 \rho - 0.00494 \rho^2, \\ Y_e &= 0.07663 + 0.0138 \rho - 5.99 \times 10^{-4} \rho^2, \end{aligned} \quad (13)$$

for $\rho \sim (6.92 \times 10^{11} - 8.04 \times 10^{14})$ and $(8.04 \times 10^{14} - 2.69 \times 10^{15})$ g cm $^{-3}$, respectively. At the midpoint of 8.04×10^{14} g cm $^{-3}$, the "jump" of Y_e is about 4×10^{-3} , and its relative variation $\sim 3.7\%$, which also ensures the continuities of two expressions above. The typical differences between the fit and the data are $10^{-3} - 10^{-4}$, and their relative differences are typically 10^{-3} .

In the same way, we calculate the values of the related quantities for NL3 parameter set. The analytical expressions of Y_e and ρ for NL3 parameter set are given as

$$\begin{aligned} Y_e &= -0.00436 + 0.0749 \rho - 0.00851 \rho^2, \\ Y_e &= 0.11556 + 0.00931 \rho - 3.52 \times 10^{-4} \rho^2, \end{aligned} \quad (14)$$

for $\rho \sim (5.69 \times 10^{11} - 7.42 \times 10^{14})$ and $(7.42 \times 10^{14} - 2.71 \times 10^{15})$ g cm $^{-3}$, respectively. At the midpoint of 7.42×10^{14} g cm $^{-3}$, the "jump" of Y_e is about 3.4×10^{-3} , and its relative variation $\sim 2.5\%$, which also ensures the continuities of two expressions above. The maximum absolute deviation and relative error are 3.5×10^{-3} and 2%, respectively, at the high-density end.

Using Equations.(13-14) and Equation (1), we obtain the fitted values of $E_F(e)$ for both NL3 and GM1(SU3) parameter sets. Figure 2(c-f) shows comparisons of the EoS of the two parameter sets and their analytical representations. In Figure 2, the data points are rarefied, and the dots and lines are for the data and the fit, respectively. It is also obvious that the analytic results agrees well with the data obtained from these three parameter sets.

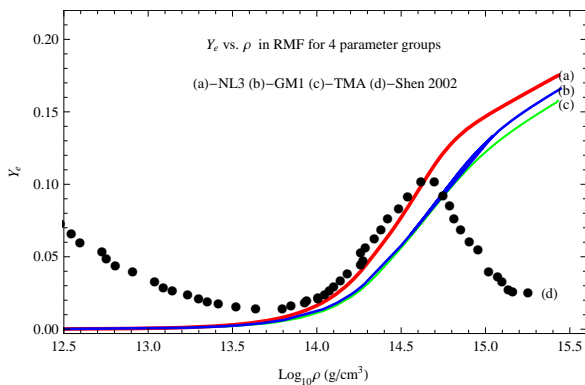


Fig. 2 Comparing Y_e vs. ρ of in RMF for 4 parameter groups.

In order compare the three parameter sets, we plot the diagrams of Y_e and ρ for RMF models in Fig.3. In the figure, the added red-dot-line is fitted from the work of Shen (2002). The author constructed the EoS in a wide NS density range using RMF theory. At lower densities, the Thomas-Fermi approximation was used to describe the

nonuniform matter composed of a lattice of heavy nuclei; while at higher densities, the TM1 parameter set was adopted. Thus, Y_e firstly increased, then decreased with ρ . However, the inclusion of hyperons softened the EoS considerably at high densities, the maximum stellar mass in Shen (2002) was estimated about $1.6 M_{\text{Sun}}$, (due to the depression of hyperons on Fermions), which deviates from the observational NS mass (Demorest et al. 2010).

4 Discussion and conclusions

In summary, we have performed numerical simulations firstly in APR98, then in relativistic mean field models, and obtained several analytical representations of Y_e . Since Y_e and $E_F(e)$ are important in assessing cooling rate of a NS and the possibility of kaon/pion condensation in the NS interior, the analytical representations obtained will be very useful in the future study on thermal evolution of a NS and the EoS of NS matter under extreme conditions, though our methods are indeed simple.

Acknowledgements. This work was supported by National Basic Research Program of China grants 973 Programs 2015CB857100, the West Light Foundation of CAS through grants XBBS-2014-23, XBBS-2014-22 and 2172201302, Chinese National Science Foundation through grants No.11673056,11622326, 11273051,11373006, 11133004 and 11173042, the Strategic Priority Research Program of CAS through XDB23000000 and National Program on Key Research and Development Project through No. 2016YFA0400803.

References

- Akmal, A., Pandharipande, V. R., & Ravenhall, D. G. 1998, Phys. Rev. C, 58, 1804.
- Baym, G., Pethick, R., & Sutherland, P. 1971, ApJ, 171, 299.
- Cheng, Q., Yu, Y.-W., & Zheng, X.-P. 2015, MNRAS, 454, 2299.
- Cheng, Q., Zhang, S.-N., & Zheng, X.-P. 2017a, RAA, 17, 054.
- Cheng, Q., Zhang, S.-N., & Zheng, X.-P. 2017b, Phys. Rev. D, 95, 083003.
- Dong, J. M., Lombardo, U., & Zuo, W. 2013, Phys. Rev. C, 87, 062801.
- Dong, J. M., Lombardo, U., Zhang, H. F., & Zuo, W. 2016, ApJ, 817, 6.
- Douchin, F., & Haensel, P. 2000, Phys. Lett. B, 485, 107.
- Douchin, F., & Haensel, P. 2001, A&A, 380, 151.
- Dutra, M., Lourenço, O., Avancini, S. S., et al.: 2014, Phys. Rev. C, 90, 055203.
- Demorest, P. B., Pennucci, T., Ransom, S. M., Roberts, M. S. E., & Hessels, J. W. T. 2010, Nature, 467, 1081.
- Gao, Z. F., Wang, N., Yuan, J. P., et al. 2011a, Ap&SS, 333, 427.
- Gao, Z. F., Wang, N., Song, D. L., Yuan, J. P., & Chou, C.-K. 2011b, Ap&SS, 334, 281.
- Gao, Z. F., Wang, N., Xu, Y., Shan, H., & Li, X.-D. 2015, Astron. Nachr., 336, 866.
- Gao, Z. F., Li, X.-D., Wang, N., et al. 2016, MNRAS, 456, 55.
- Gao, Z.-F., Wang, N., Shan, H., et al. 2017, ApJ, 849, 19.
- Geng, L., Toki, H., Meng, J. 2005, Progr. Theor. Phys., 113, 785
- Glendenning, N. K., 1985, ApJ, 293, 470.
- Gomes, R. O., Dexheimer, V., & Vasconcellos, C. A. Z. 2014, Astron. Nachr., 335, 666.

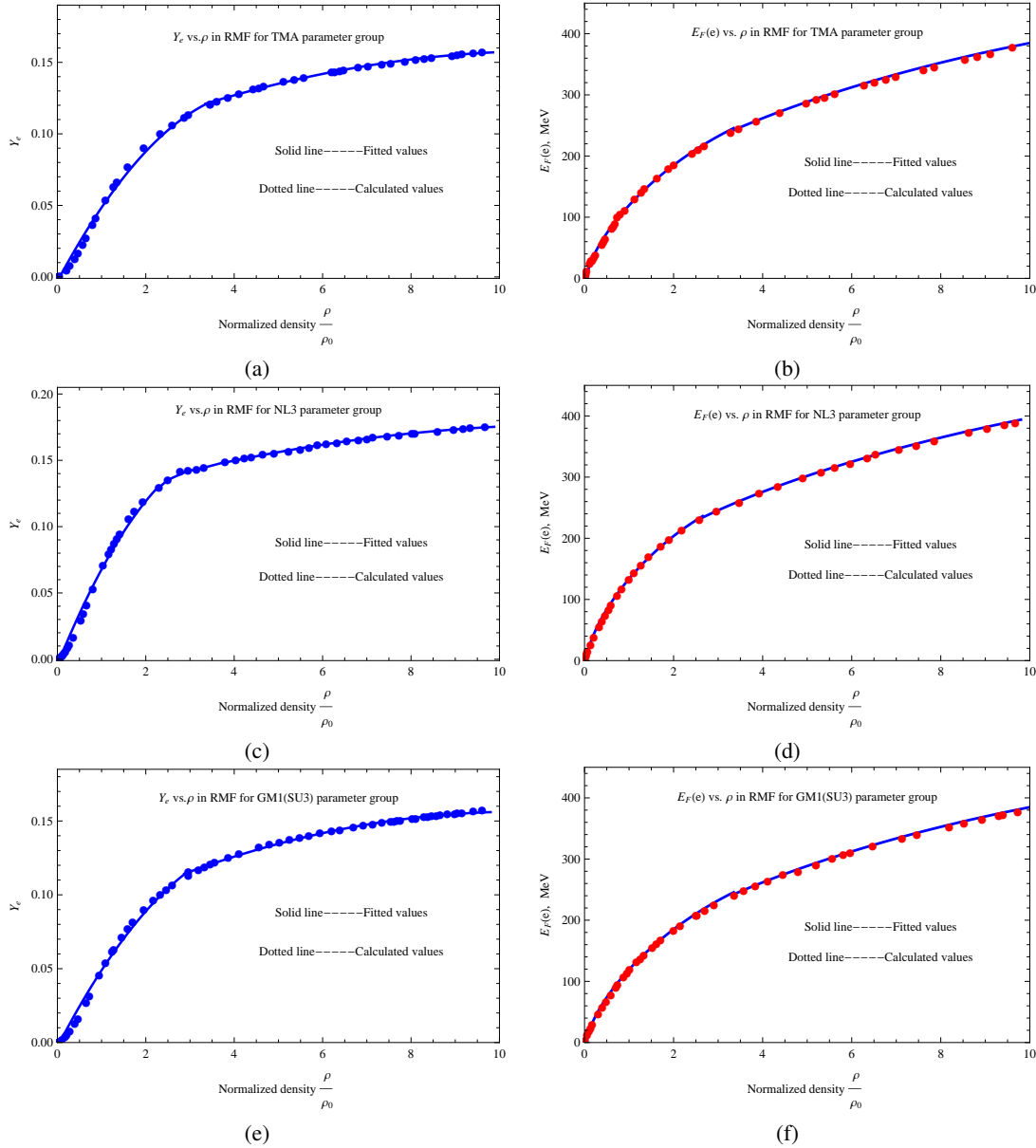


Fig. 3 Numerically fitting in RMF within TMA, NL3 and GM1(SU3) parameter sets. Left (a), (c), (e), the relations of Y_e and ρ . Bottom, (b), (d), (f), the relation of $E_F(e)$ and ρ . Top, center and bottom are for TMA, NL3 and GM1(SU3) parameter sets, respectively.

Gomes, R. O., Franzon, B., Dexheimer, V., & Schramm, S. 2017, *ApJ*, 850, 20.
 Graber, V., Andersson, N., Glampedakis, K., & Lander, Samuel K. 2015, *MNRAS*, 453, 671.
 Graber, V., Andersson, N., & Hogg, M. 2017, *Int. J. Mod. Phys. D.*, 26, 1730015.
 Kaminker, A. D., Kaurov, A. A., Potekhin, A. Y., & Yakovlev, D. G. 2014, *MNRAS*, 442, 3484.
 Lattimer, J. M., & Prakash, M. 2007, *Phys. Rep.*, 442, 109.
 Lalazisis, G. A., König, J., & Ring, P. 1997, *Phys. Rev. C*, 55, 540.
 Li, X. H., Gao, Z. F., Li, X. D., et al. 2016, *Int. J. Mod. Phys. D.*, 25, 1650002.
 Liu, J.-J. 2016, *RAA*, 16, 83, arXiv:1602.05501

Liu, J.-J., et al. 2016, *RAA*, 16, 174
 Liu, J.-J., Peng, Q.-H., Hao, L.-H., et al. 2017a, *RAA*, 17, 107.
 Liu, J.-J., Peng, Q.-H., & Liu, D.-M. 2017b, *Chin Phys. C.*, 41, 095101, arXiv:1701.05771
 Liu, J.-J., & Liu, D.-M. 2017a, *ChPhC*, arXiv:1701.01088
 Liu, J.-J., & Liu, D.-M. 2017b, *RAA*, arXiv:1711.01955
 Mu, X., Jia, H., Zhou, X., & Wang, H. 2017, *ApJ*, 846, 140.
 Potekhin, A. Y., Fantina, A. F., Chamel, N., Pearson, J. M., & Goriely, S. 2013, *A&A*, 560, 48.
 Schaffner, J., & Mishustin, I. N. 1996, *Phys. Rev. C*, 33, 1416.
 Shen, H. 2002, *Phys. Rev. C*, 65, 035802.
 Sun, X.-D., Guo, P., Li, X.-H. 2016, *Phys. Rev. C*, 93, 034316.
 Stoks, V. G. J., Klomp, R. A. M., Rentmeester, M. C. M., & de Swart, J. J. 1993, *Phys. Rev. C*, 48, 792.

- Toki, H., Hirata, D., Sugahara, Y., Sumiyoshi, K., & Tanihata, I. 1995, Nucl. Phys. A, 588, 357.
- Xia, C.-J., Peng, G.-X., Zhao, En-Guang; Zhou, Shan-Gui et al. 2016, Phys. Rev. D, 93, 085025.
- Xia, C.-J., & Zhou, S.-G. 2017, Nucl. Phys. B, 916, 669.
- Xu, Y., et al. 2012, Chin. Phys. Lett., 29, 059701.
- Yakovlev, D. G., et al. 2001, Phys. Rep, 354, 1.
- Yang, F., & Shen, H., 2008, Phys. Rev. C, 77, 025801.
- Zhao, X.-F. 2015, Int. J. Mod. Phys. D., 24, 1550058
- Zhao, X.-F. 2016, Chinese Journal of Physics, 54, 839.
- Zhu, C., Gao, Z. F., Li, X. D., et al. 2016, Mod. Phys. Lett. A, 31, 1650070.
- Zhou, X., Jia, H., Hong, B., Mu, X., & Wang, H. 2017, Int. J. Mod. Phys. D., 26, 1750077.